Current-Nonlinear Hall Effect and Spin-Orbit Torque Magnetization Switching in a Magnetic Topological Insulator

K. Yasuda, A. Tsukazaki, R. Yoshimi, K. Kondou, K. S. Takahashi, Y. Otani, M. Kawasaki, and Y. Tokura

Phys. Rev. Lett. **119**, 137204 — Published 28 September 2017

DOI: 10.1103/PhysRevLett.119.137204

Current-nonlinear Hall effect and spin-orbit torque magnetization switching in a magnetic topological insulator

K. Yasuda,[1,*] A. Tsukazaki,[2] R. Yoshimi,[3] K. Kondou,[3] K. S. Takahashi,[3] Y. Otani,[3,4] M. Kawasaki,[1,3] and Y. Tokura[1,3]

[1] *Department of Applied Physics and Quantum-Phase Electronics Center (QPEC), University of Tokyo, Tokyo 113-8656, Japan*
[2] *Institute for Materials Research, Tohoku University, Sendai 980-8577, Japan*
[3] *RIKEN Center for Emergent Matter Science (CEMS), Wako 351-0198, Japan*
[4] *Institute for Solid State Physics (ISSP), University of Tokyo, Kashiwa 277-8581, Japan*

(Dated: August 14, 2017)

Current-nonlinear Hall effect or second harmonic Hall voltage is widely used as one of the methods for estimating charge-spin conversion efficiency, which is attributed to the magnetization oscillation by spin-orbit torque (SOT). Here, we argue the second harmonic Hall voltage under large in-plane magnetic field with in-plane magnetization configuration in magnetic/nonmagnetic topological insulator (TI) heterostructures, $Cr_x(Bi_{1-y}Sb_y)_{2-x}Te_3/(Bi_{1-y}Sb_y)_2Te_3$, where it is clearly shown that the large second harmonic voltage is governed not by SOT but mainly by asymmetric magnon scattering without macroscopic magnetization oscillation. Thus, this method does not allow an accurate estimation of charge-spin conversion efficiency in TI. Instead, the SOT contribution is exemplified by current pulse induced non-volatile magnetization switching, which is realized with current density of 2.5×10^{10} A m^{-2}, showing its potential as spintronic materials.

PACS numbers: 72.10.Di, 77.80.Fm, 75.47.-m, 85.75.-d

Interconversion of angular momentum between conduction electron and local magnetization is one of the central issues of contemporary spintronic research. For example, in normal metal/ferromagnet (NM/FM) heterostructures, spin-orbit torque (SOT) due to the spin current generated by the spin Hall effect in NM plays a key role in manipulating the magnetization of FM [1, 2]. This enables magnetization switching [3–6] as well as fast domain wall motion [7, 8], which directly leads to computation, logic and memory device applications. In particular, materials with large charge-spin conversion efficiency θ_{CS} can provide large spin current with minimal Joule heating enabling energy-saving spintronic devices in the future. Reflecting the importance of an accurate estimation of θ_{CS}, several techniques have recently been developed such as spin pumping [9, 10], spin torque ferromagnetic resonance (ST-FMR) [5, 6, 11–14] and second harmonic Hall voltage measurement [15–19]. Utilizing these methods, three-dimensional topological insulators (TI) have been demonstrated to have quite a large θ_{CS} [10, 12–14, 18, 19].

TI is a class of materials with insulating bulk and conductive surface state with Dirac dispersion [20]. The spin direction of the surface electron is locked to its momentum, termed "spin-momentum locking", which makes TI an ideal spintronic material with large θ_{CS} [10, 12–14, 18, 19]. Moreover, magnetic TI provides one of the ideal platforms to exemplify the spin-polarized electron transport interacting with underlying magnetism [18, 19, 21–25]. In fact, large current-direction-dependent or unidirectional magnetoresistance (UMR) [26–30] is observed under appropriate magnetization and current directions [25]. Such current-nonlinear longitudinal resistance is attributed to the asymmetric scattering of conduction electron by magnon due to the conservation of angular momentum, what we call "asymmetric magnon scattering mechanism" [25].

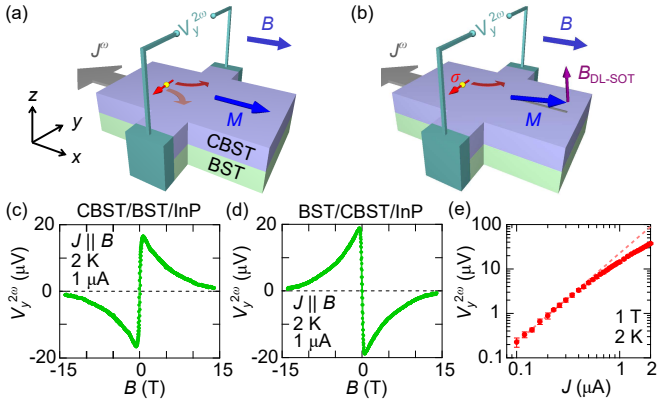

FIG. 1. (a), Schematic illustration of second harmonic Hall voltage $V_y^{2\omega}$ caused by J^2-proportional nonlinear conduction in CBST/BST. Nonlinear conduction results in finite $V_y^{2\omega}$ at $M \parallel J$ configuration even if macroscopic magnetization is not tilted. (b), Schematic illustration of $V_y^{2\omega}$ caused by magnetization tilting due to the effective field by damping-like spin-orbit torque. External magnetic field B and ac current J^ω are applied in parallel. Magnetization M is tilted by the effective field due to DL-SOT $B_{DL\text{-}SOT}$ caused by the spin accumulation σ. (c), Magnetic field dependence of $V_y^{2\omega}$ at 2 K and 1 μA for the CBST/BST/InP sample. (d), The same as (c) for the inverted sample, BST/CBST/InP. (e), Current magnitude J dependence of $V_y^{2\omega}$ at 2 K and 1 T for the CBST/BST/InP sample. The dotted line represents $V_y^{2\omega} \propto J^2$.

In this paper, we reveal that the asymmetric magnon scattering mechanism gives rise to current-nonlinear re-

sistance also in the transverse direction in magnetic TI under certain configuration, which is observed as the large second harmonic Hall voltage. Importantly, the present result means that $\theta_{\rm CS}$ cannot be accurately evaluated by second harmonic technique because the second harmonic voltage is governed not by SOT but mainly by asymmetric magnon scattering. As a target material, we characterize TI heterostructures [18, 24, 25, 31] composed of nonmagnetic TI $(Bi_{1-y}Sb_y)_2Te_3$ (BST) [32, 33] and magnetic TI $Cr_x(Bi_{1-y}Sb_y)_{2-x}Te_3$ (CBST) [21–23] grown on semi-insulating InP substrate with molecular beam epitaxy (MBE) with negligible diffusion of Cr [24, 31] and tuned Fermi energy $E_{\rm F}$ to the surface state in the bulk band gap [32] (see Supplemental Material S1). Hence, only top and bottom surfaces are conductive as can be seen from the observation of quantum Hall effect under high perpendicular magnetic field (see Supplemental Material S2) [31]. Here, the second harmonic voltage is expected only from one surface involved in the Cr-doped magnetic layer, which would be otherwise canceled out by the opposite contributions of two surfaces [24, 25].

Anomalous Hall voltage is usually proportional to current J and out-of-plane component of magnetization M_z. In addition, at $J \parallel M \parallel x$ configuration in the heterostructure under large in-plane magnetic field $B \parallel x$, an additional nonlinear transverse voltage proportional to J^2 is allowed from symmetry [Fig. 1(a)]. Here, the transverse voltage is expressed as,

$$V_y = R_{\rm AHE} J_x M_z + R^{(2)}_{yx} J_x^2, \tag{1}$$

where $R^{(2)}_{yx}$ is a coefficient. Note that we can neglect ordinary Hall effect and planar Hall effect since they are prohibited in the present experimental configuration [16]. The first term, corresponding to anomalous Hall voltage, becomes zero when M is pointing along the in-plane direction (x). When a large current is applied, however, M is tilted to the out-of-plane direction by damping-like SOT (DL-SOT) [1, 2, 16] as shown in Fig. 1(b) so that $M_z = c_{\rm DL\text{-}SOT} J_x$, where $c_{\rm DL\text{-}SOT}$ is a proportional constant. This is because the effective field by DL-SOT ($B_{\rm DL\text{-}SOT}$) is directed along $\sigma \times M$ [4], where σ is the spin accumulation direction due to the Rashba-Edelstein effect at the top surface state [34]. Therefore, under large current and $J \parallel B \parallel x$ configuration, the Hall voltage is expressed as,

$$V_y = R_{\rm AHE} c_{\rm DL\text{-}SOT} J_x^2 + R^{(2)}_{yx} J_x^2. \tag{2}$$

Both of these two terms are proportional to J^2 (current-nonlinear) but the physical meaning is completely different; M is tilted by the DL-SOT mechanism whereas macroscopic M is unaffected in nonlinear conduction. Only when the second term in equation (2) is negligible, $V_y = R_{\rm AHE} c_{\rm DL\text{-}SOT} J_x^2$ allows us to estimate $B_{\rm DL\text{-}SOT}$

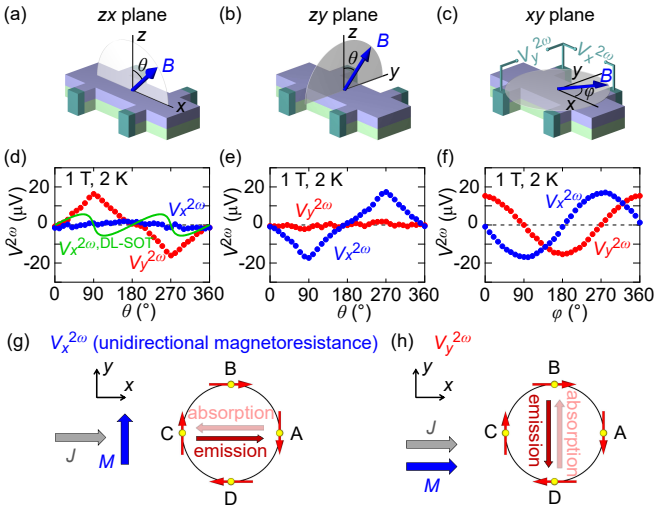

FIG. 2. (a)-(c), Schematic illustrations of measurement configurations for angular dependence. (d)-(f), Angular dependence of second harmonic longitudinal voltage $V_x^{2\omega}$ and second harmonic transverse (Hall) voltage $V_y^{2\omega}$ for zx plane (d), zy plane (e) and xy plane (f). The measurements were done at 2 K, 1 T and 1 μA. The green line $V_x^{2\omega,\rm DL\text{-}SOT}$ illustrates the theoretically calculated second harmonic voltage based on the assumption that $V_y^{2\omega}$ originated purely from the DL-SOT mechanism with magnetization oscillation. (g), Illustration of the origin of $V_x^{2\omega}$ under $J \perp M$ configuration. Red and pink arrows represent the scatterings by magnon emission and absorption processes at around the Fermi surface, respectively. (h), Illustration of the origin of $V_y^{2\omega}$ under $J \parallel M$ configuration.

through the second harmonic Hall voltage [15–19] or current-direction-dependent Hall resistance [4, 5].

For a second harmonic Hall voltage measurement, we put ac current $J^\omega = J\sin(\omega t)$ in the x direction into the Hall bar, then the transverse voltage $V_y = (R_{\rm AHE} c_{\rm DL\text{-}SOT} + R^{(2)}_{yx})(\frac{J^2}{2} - \frac{J^2}{2}\cos(2\omega t))$ appears, which is measured with lock-in techniques (see Supplemental Material S1). Figure 1(c) shows the magnetic field dependence of second harmonic Hall voltage $V_y^{2\omega}$ for the CBST(3 nm)/BST(5 nm)/InP film. At around $B = 0$ T, $V_y^{2\omega}$ changes its sign with a small hysteresis associated with the magnetization reversal, forming the out-of-plane multidomain state due to the strong perpendicular magnetic anisotropy [18, 25] (see Supplemental Material S3). As magnetic field is applied up to ~ 0.7 T, magnetization becomes single domain pointing along x direction. Hereafter, we only discuss the $V_y^{2\omega}$ signal above 0.7 T to avoid the difficulty in interpretation due to the multidomain formation. In the inverted heterostructure, BST(3 nm)/CBST(5 nm)/InP, the sign of $V_y^{2\omega}$ is reversed while showing a comparable magnitude as shown in Fig. 1(d). This is because the manner of the spin-momentum locking is opposite between the two surfaces [25]. In addition, we can eliminate thermoelectric effects such as anomalous Nernst effect or spin Seebeck effect as the dominant

origin of $V_y^{2\omega}$, because the heat gradient and the resultant thermoelectromotive force provide the contribution of the same sign in both heterostructures when InP substrate works as a heat bath [25] and the resistance of the BST and CBST surfaces are comparable (∼30 kΩ per one surface at around 2 K [21–23, 32, 33]). As shown in Fig. 1(e), $V_y^{2\omega}$ is proportional to J^2 at low current amplitude as expected from equation (2). The deviation from the proportionality at larger current originates from heating [25]. When we assume that $V_y^{2\omega}$originates only from the DL-SOT mechanism, the effective field $B_{\text{DL-SOT}}$ would amount to ∼ 26 mT under $J = 1$ μA. Also, the charge-spin conversion efficiency $\theta_{\text{CS}} = j_{\text{S}}/j_{\text{C}}$ would amount to ∼ 160, where j_{S} (j_{C}) is the spin (charge) current density (see Supplemental Material S4). The estimated θ_{CS} is comparable to that deduced by the previous second harmonic Hall measurements (θ_{CS} : 80 - 425) [18, 19] and extraordinarily larger than estimations by ST-FMR or spin pumping (θ_{CS} : 0.4 - 3.5) [10, 12–14]. As shown in the following, we argue against the extraordinary value of θ_{CS} as derived from the observed large $V_y^{2\omega}$.

To examine the origin of the large $V_y^{2\omega}$ signal, we measured magnetic-field direction dependence of second harmonic longitudinal voltage $V_x^{2\omega}$ and Hall (transverse) voltage $V_y^{2\omega}$ in CBST/BST/InP as shown in Figs. 2(a)-(f). First, one can say that the effective field by field-like SOT (FL-SOT) and Oersted field are not the main origin of $V_y^{2\omega}$: If these fields were dominant, $V_y^{2\omega}$ would be finite in zy plane [16] since they point in the y direction. Next, let us assume that $V_y^{2\omega}$ originated purely from magnetization oscillation by DL-SOT. In this case, $V_x^{2\omega}$ in Fig. 2(d) should become non-zero as well, because longitudinal resistance R_{xx} depends on the magnetization direction; R_{xx} amounts to 16.4 kΩ (15.6 kΩ) when $M \parallel z$ ($M \parallel x$). If M were oscillating in the zx plane, it would modulate longitudinal resistance as well as anomalous Hall resistance so that $V_x^{2\omega}$ should also show a finite value [17]. Here, the calculated signal from DL-SOT $V_x^{2\omega,\text{DL-SOT}}$ is shown with the green line in Fig. 2(d) (see Supplemental Material S5). The experimental $V_x^{2\omega}$ (blue line in Fig. 2(d)), however, does not show such a feature of $V_x^{2\omega,\text{DL-SOT}}$ signal, meaning that the original assumption is incorrect. Therefore, we can conclude that DL-SOT contributes little to $V_x^{2\omega}$ and hence to $V_y^{2\omega}$; namely $V_y^{2\omega}$ should originate mainly from nonlinear conduction (the second term in equation (2)).

To elucidate the origin of nonlinear conduction, we note that $V_y^{2\omega}$ and $V_x^{2\omega}$ have the same order of magnitude with a phase shift of 90 degrees as shown in Fig. 2(f) (see also Supplemental Material S6), which indicates the same microscopic origin of $V_x^{2\omega}$ and $V_y^{2\omega}$. In Figs. 2(d)-(f), $V_x^{2\omega}$ is maximum when $M \perp J$. This is nothing but UMR [25–30], which comes from the second term of $V_x = R_{xx}J_x + R_{xx}^{(2)}J_x^2$ [25]. Here, the J^2-proportional voltage derives from the asymmetric relaxation time between the electron with positive group velocity (position A) and that with negative group velocity (C) as shown in Fig. 2(g) [25]: The scattering processes by magnon are inequivalent between A and C due to spin-momentum locking and conservation of angular momentum [25, 29, 30]. In a similar manner, the J^2-proportional transverse voltage ($R_{yx}^{(2)}J_x^2$ in equations (1) and (2)) can be derived when $M \parallel J$ as shown in Fig. 2(h). When electron with positive group velocity (at around position B, angular momentum $+1/2$ with the quantization direction is taken along $x \parallel M$) is scattered to around D (momentum $-1/2$), the process accompanies the emission of magnon with the angular momentum of $+1$. On the other hand, the scattering of electron with negative group velocity (at around D, $-1/2$) to around B ($+1/2$) must absorb magnon. This nonequivalence in scattering processes leads to the asymmetry in relaxation time and eventually to that in the electron distribution between around D and around B under non-equilibrium condition, which is the origin of the J^2-proportional transverse term (nonlinear conduction). Such asymmetric magnon scattering model allows us to evaluate $R_{yx}^{(2)}$ (see Supplemental Material S7). From that model, we can analytically show that $V_x^{2\omega}(J \parallel x, M \parallel y) = -3V_y^{2\omega}(J \parallel x,\ M \parallel x)$; namely $V_x^{2\omega}$ and $V_y^{2\omega}$ show the same order of magnitude, consistent with the experimental results including their signs (see Supplemental Material S8). The quantitative deviation of the ratio $V_x^{2\omega}/V_y^{2\omega}$ between the calculation and the experiment originates from the approximations adopted in the calculation such as relaxation time approximation, simplified band and magnon dispersions [25].

To further examine the validity of the asymmetric magnon scattering model, we calculate the temperature

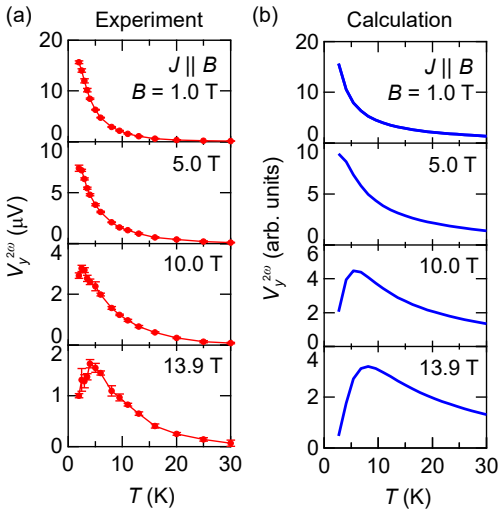

FIG. 3. (a), Observed temperature dependence of $V_y^{2\omega}$ under various magnetic fields at 1 μA under $J \parallel B$ configuration. (b), Numerical calculation results of temperature dependent $V_y^{2\omega}$.

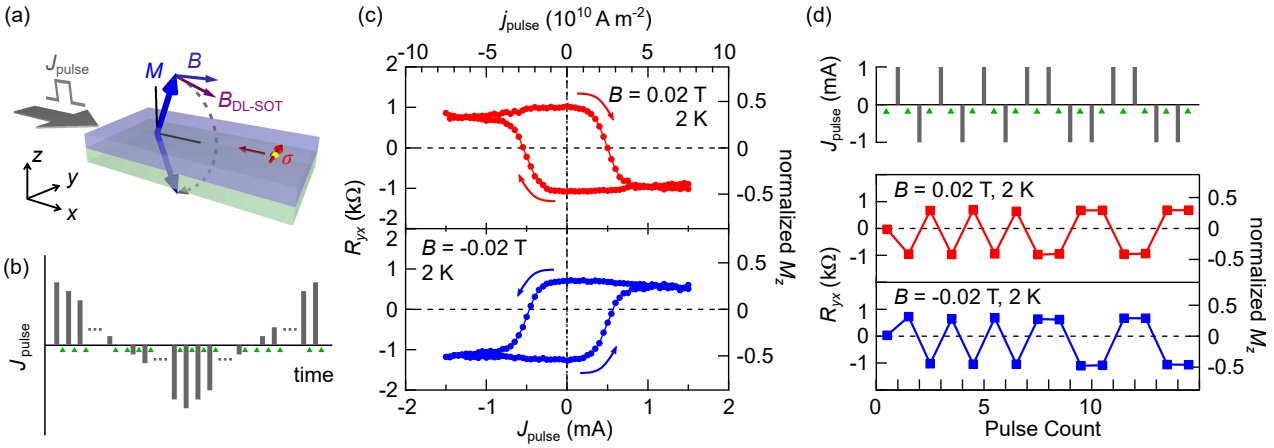

FIG. 4. (a), Schematic illustration of current-pulse-induced magnetization switching. (b), Schematic of measurement procedure. Hall resistance is measured under low current (~ 1 μA) at the green triangle every time after current pulse injection as shown in the gray bar. The current pulse $J_{\rm pulse}$ is applied in the positive, negative and then positive direction with gradually changing its magnitude. (c), Current pulse amplitude $J_{\rm pulse}$ dependence of Hall resistance R_{yx} under in plane magnetic field $B = \pm 0.02$ T at 2 K. The corresponding current pulse density $j_{\rm pulse}$ is shown on the upper abscissa. The normalized M_z, calculated as $R_{yx}/R_{\rm AHE}$, is shown in the right scale, where $R_{\rm AHE} = 2.3$ kΩ. This corresponds to $(r_{\rm up} - r_{\rm down})/(r_{\rm up} + r_{\rm down})$, where $r_{\rm up}$ ($r_{\rm down}$) is the fraction of up (down) domain. (d), Repeated magnetization switching under $B = \pm 0.02$ T and $J_{\rm pulse} = \pm 1$ mA at 2 K. Prior to the first current pulse, magnetization is initialized to the multidomain state with zero net M_z.

and magnetic field dependence of $V_y^{2\omega}$ and compare with the experimental results in Fig. 3. The experiment and the calculation show qualitative consistency; $V_y^{2\omega}$ monotonically decreases as raising temperature at low magnetic fields (B =1 T and 5 T) and almost vanishes at around $T_c \sim 34$ K. On the other hand, $V_y^{2\omega}$ at a high magnetic field (13.9 T) shows a peak structure. These behaviors are similar to those observed in UMR (or $V_x^{2\omega}$ [25]. According to the asymmetric magnon scattering model, such a change in the energy scale as a function of magnetic field B can be explained by the variation of the magnon gap ($\sim g\mu_B B$), where g and μ_B are g factor and Bohr magneton, respectively. In contrast, the peak behaviors at high magnetic fields cannot be explained by the DL-SOT-based model, since DL-SOT has no characteristic energy scale [2]. Also, the field induced suppression of $V_y^{2\omega}$ is well reproduced in the calculation, which is attributed to the decrease of the magnon population due to the gap opening at high fields [25]. Therefore, the results again support the asymmetric magnon scattering origin of $V_y^{2\omega}$, namely $R_{\rm AHE}c_{\text{DL-SOT}} \ll R_{yx}^{(2)}$, which leads to the overestimation of $\theta_{\rm CS}$ in magnetic TI [18, 19].

Then, in what current region and how can the effect of DL-SOT show up for the present TI heterostructure? Note here that the above argument of nonlinear Hall effect is applicable not only to the ac current measurement but also to the dc current one. Since $R_{\rm AHE}c_{\text{DL-SOT}} \ll R_{yx}^{(2)}$, the Hall resistance measured under dc current and large in-plane magnetic field becomes $R_{yx} = V_y/J_x \simeq R_{yx}^{(2)}J_x$. Such current-direction-dependent Hall resistance due to the asymmetric magnon scattering is hard to distinguish from DL-SOT contribution [18, 19]. To avoid this difficulty, the non-volatile magnetization switching has to be examined directly by current pulse injection, but not by Hall resistance measurement under large dc current. Figure 4(a) shows the schematic illustration of current-pulse induced magnetization switching experiment; current pulse $J_{\rm pulse}$ is injected parallel to the in-plane external magnetic field B. Here, the effective field $B_{\text{DL-SOT}}$ rotates the magnetization with the assistance of small in-plane B, which is required to define the switching direction. As shown in Fig. 4(b), after every current pulse injection (gray bar), the possible change in M_z is evaluated though Hall resistance R_{yx} measured with low current (1 μA, green triangle) [3] (see Supplemental Material S1). Here, the asymmetric magnon scattering is negligible because its contribution of ~ 10 μV is much smaller than the anomalous Hall voltage of ~ 1 mV. Figure 4(c) shows R_{yx}-$J_{\rm pulse}$ loops at 2 K under in-plane magnetic field $B = \pm 0.02$ T. Note that 0.02 T is much smaller than anisotropy field 0.7 T and therefore magnetization is pointing almost exclusively up or down. Thus, the intermediate value of R_{yx} or normalized M_z indicates the multidomain formation. As clearly seen in Fig. 4(c), R_{yx} is switched from negative (positive) to positive (negative) at around $J_{\rm pulse} = -0.5$ mA (+0.5 mA) under B =0.02 T, pointing to the current induced magnetization reversal. The switching direction is reversed under $B = -0.02$ T. Furthermore, the magnetization direction can be repeatedly controlled by current injection of ± 1 mA as shown in Fig. 4(d). From these experiments, we can conclude that the switching is caused by DL-SOT (Fig. 4(a)) since the effective field by FL-

SOT and Oersted field along y direction cannot make a deterministic switching in this configuration. We note that the magnetization switching ratio (normalized M_z) is limited to ~ 0.4, which is relatively small compared with the full switching operation in NM/FM heterostructures [3–6], whose origin is yet to be clarified. The threshold current $J_{\rm th}$ =0.5 mA corresponds to current density of 2.5×10^{10} A m^{-2}. In spite of the larger perpendicular anisotropy, the threshold current density is still much smaller than those (10^{11} - 10^{12} A m^{-2}) of NM/FM heterostructures [3–6]. This can be attributed to the smaller saturation magnetization $M_{\rm s} = 3.5 \times 10^4$ A m^{-1} (Joule heating by current pulse injection may further assist the switching through the decrease of $M_{\rm s}$) as well as to the larger $\theta_{\rm CS}$ of TI [10, 12–14], showing a high potential of the TI heterostructures as spintronic materials.

We thank S. Seki, F. Kagawa, H. Oike and M. Kawamura for fruitful discussions. K. Y. is supported by the Japan Society for the Promotion of Science (JSPS) through a research fellowship for young scientists (No. 16J03476). This research was supported by the Japan Society for the Promotion of Science through the Funding Program for World-Leading Innovative R & D on Science and Technology (FIRST Program) on "Quantum Science on Strong Correlation" initiated by the Council for Science and Technology Policy and by JSPS Grant-in-Aid for Scientific Research(S) No. 24224009 and No. 24226002 and No. JP15H05853 from MEXT, Japan. This work was also supported by CREST, JST.

* yasuda@cmr.t.u-tokyo.ac.jp

[1] J. C. Slonczewski, J. Magn. Magn. Mat. **159**, L1 (1996).
[2] D. C. Ralph, and M. D. Stiles, J. Mag. Mag. Mat. **230**, 1190 (2008).
[3] I. M. Miron, K. Garello, G. Gaudin, P. J. Zermatten, M. V. Costache, S. Auffret, S. Bandiera, B. Rodmacq, A. Schuhl, and P. Gambardella, Nature **476**, 189 (2011).
[4] L. Liu, O. J. Lee, T. J. Gudmundsen, D. C. Ralph, and R. A. Buhrman, Phys. Rev. Lett. **109**, 096602 (2012).
[5] L. Liu, C. F. Pai, Y. Li, H. W. Tseng, D. C. Ralph, and R. A. Buhrman, Science **336**, 555 (2012).
[6] C. F. Pai, L. Liu, Y. Li, H. W. Tseng, D. C. Ralph and R. A. Buhrman, Appl. Phys. Lett. **101**, 122404 (2012).
[7] S. Emori, U. Bauer, S. M. Ahn, E. Martinez, and G. S. D. Beach, Nat. Mater. **12**, 611 (2013).
[8] K. S. Ryu, L. Thomas, S. H. Yang, and S. Parkin, Nat. Nanotech. **8**, 527 (2013).
[9] O. Mosendz, J. E. Pearson, F. Y. Fradin, G. E. W. Bauer, S. D. Bader, and A. Hoffmann, Phys. Rev. Lett. **104**, 046601 (2010).
[10] M. Jamali, J. S. Lee, J. S. Jeong, F. Mahfouzi, Y. Lv, Z. Zhao, B. K. Nikolić, K. A. Mkhoyan, N. Samarth, and J. P. Wang, Nano Lett. **15**, 7126 (2015).
[11] L. Liu, O. J. Lee, T. J. Gudmundsen, D. C. Ralph, and R. A. Buhrman, Phys. Rev. Lett. **109**, 096602 (2012).
[12] A. R. Mellnik *et al.*, Nature **511**, 449 (2014).
[13] Y. Wang, P. Deorani, K. Banerjee, N. Koirala, M. Brahlek, S. Oh, and H. Yang, Phys. Rev. Lett. **114**, 257202 (2015).
[14] K. Kondou, R. Yoshimi, A. Tsukazaki, Y. Fukuma, J. Matsuno, K. S. Takahashi, M. Kawasaki, Y. Tokura, and Y. Otani, Nat. Phys. **12**, 1027 (2016).
[15] J. Kim, *et al.*, Nat. Mater. **12**, 240 (2013).
[16] K. Garello, I. M. Miron, C. O. Avci, F. Freimuth, Y. Mokrousov, S. Blgel, S. Auffret, O. Boulle, G. Gaudin, and P. Gambardella, Nat. Nanotech. **8**, 587 (2013).
[17] M. Hayashi, J. Kim, M. Yamanouchi, and H. Ohno, Phys. Rev. B **89**, 144425 (2014).
[18] Y. Fan *et al.*, Nat. Mater. **13**, 699 (2014).
[19] Y. Fan *et al.*, Nat. Nanotech. **11**, 352 (2016).
[20] M. Z. Hasan, and C. L. Kane, Rev. Mod. Phys. **82**, 3045 (2010).
[21] C. Z. Chang *et al.*, Science **340**, 167 (2013).
[22] J. G. Checkelsky, R. Yoshimi, A. Tsukazaki, K. S. Takahashi, Y. Kozuka, J. Falson, M. Kawasaki, and Y. Tokura, Nat. Phys. **10**, 731 (2014).
[23] X. Kou *et al.*, Phys. Rev. Lett. **113**, 137201 (2014).
[24] K. Yasuda, R. Wakatsuki, T. Morimoto, R. Yoshimi, A. Tsukazaki, K. S. Takahashi, M. Ezawa, M. Kawasaki, N. Nagaosa, and Y. Tokura, Nat. Phys. **12**, 555 (2016).
[25] K. Yasuda, A. Tsukazaki, R. Yoshimi, K. S. Takahashi, M. Kawasaki, and Y. Tokura, Phys. Rev. Lett. **117**, 127202 (2016).
[26] K. Olejník, V. Novák, J. Wunderlich, and T. Jungwirth, Phys. Rev. B **91**, 180402 (2015).
[27] C. O. Avci, K. Garello, A. Ghosh, M. Gabureac, S. F. Alvarado, and P. Gambardella, Nat. Phys. **11**, 570 (2015).
[28] C. O. Avci, K. Garello, J. Mendil, A. Ghosh, N. Blasakis, M. Gabureac, M. Trassin, M. Fiebig, and P. Gambardella, Appl. Phys. Lett. **107**, 192405 (2015).
[29] S. Langenfeld, V. Tshitoyan, Z. Fang, A. Wells, T. A. Moore, and A. J. Ferguson, Appl. Phys. Lett. **108**, 192402 (2016).
[30] K. J. Kim, T. Moriyama, T. Koyama, D. Chiba, S. W. Lee, S. J. Lee, K. J. Lee, H. W. Lee, T. Ono, Preprint at https://arxiv.org/abs/1603.08746 (2016).
[31] R. Yoshimi, K. Yasuda, A. Tsukazaki, K. S. Takahashi, N. Nagaosa, M. Kawasaki, and Y. Tokura, Nat. Commun. **6**, 8530 (2015).
[32] J. Zhang *et al.*, Nat. Commun. **2**, 574 (2011).
[33] R. Yoshimi, A. Tsukazaki, Y. Kozuka, J. Falson, K. S. Takahashi, J. G. Checkelsky, N. Nagaosa, M. Kawasaki, and Y. Tokura, Nat. Commun. **6**, 6627 (2015).
[34] V. M. Edelstein, Solid State Commun. **73**, 233 (1990).
[35] Y. Zhang *et al.*, Nat. Phys. **6**, 584 (2010).